Multisite Intracellular Recordings by MEA

Micha E. Spira, Shun-Ho Huang, Nava Shmoel, and Hadas Erez

Abstract The enormous advances made over the last 50 years in materials science, microelectronics, and nanoelectronics, together with the acknowledgment that substrate-integrated planar multielectrode arrays (MEA) are limited to recording of extracellular field potentials (FPs) rather than the entire electrophysiological signaling repertoire of the brain, have prompted a number of laboratories to merge the advantages of planar MEA technologies (non-damaging and durable) with those of the classical sharp and patch electrodes for intracellular recordings. Unlike extracellular planar electrode-based MEAs, the new generation of three-dimensional (3D) vertical nanoelectrodes are designed to functionally penetrate the plasma membrane of cultured cells and operate in a similar manner to classical intracellular microelectrodes. Although only approximately 10 years has elapsed since the development of the first vertical 3D nanostructure-based MEAs, this technology has progressed to enable recordings of attenuated intracellular action potentials (APs) and synaptic potentials from individual neurons, cardiomyocytes, and striated myotubes. Furthermore, recently the scaling advantages of nanochip/microchip fabrication technologies enabled simultaneously intracellular recordings of APs from hundreds of cultured cardiomyocytes, thus heralding a new milestone in MEA technology.

In this chapter we present the earliest and today's cutting-edge achievements of this "young vertical nano-sensors MEA technology" at the single-cell and network

M. E. Spira (✉) · S.-H. Huang · N. Shmoel · H. Erez
Department of Neurobiology, The Alexander Silberman Institute of Life Science, The Hebrew University of Jerusalem, Jerusalem, Israel

The Charles E. Smith Family and Prof. Joel Elkes Laboratory for Collaborative Research in Psychobiology, The Hebrew University of Jerusalem, Jerusalem, Israel

The Harvey M. Kruger Family Center for Nanoscience, The Hebrew University of Jerusalem, Jerusalem, Israel
e-mail: Spira@cc.huji.ac.il

M. Chiappalone et al. (eds.), *In Vitro Neuronal Networks*,
Advances in Neurobiology 22, https://doi.org/10.1007/978-3-030-11135-9_5

levels, explain the biophysical principles and the various configurations used to form functional nanoelectrode/cell hybrids, and describe the quality and characteristic features of the recorded intracellular APs and subthreshold synaptic potentials by the vertical nanoelectrode-based MEA. Basic cell-biological mechanisms that curtail the length of time intracellular access by the nanoelectrodes are discussed, and approaches to overcome this problem are offered.

Recent development of biotechnologies that use induced human pluripotent stem cells taken from healthy subjects and patients, and in vitro drug screening for the development of personalized medicine as well as basic brain research will benefit tremendously from the use of MEAs that record the entire brain electrophysiological signaling repertoire from individual cells within an operational network rather than only extracellular FPs.

Keywords Intracellular recordings · Action potentials · Synaptic potentials · Electroporation · Optoporation · Seal resistance · Membrane repair · Neurons · Cardiomyocytes · Striated myotubes · Vertical nanoelectrodes · Mushroom-shaped microelectrodes

1 Introduction

Multielectrode arrays (MEA) are extensively used nowadays to study basic and applied electrophysiological aspects of in vivo and in vitro neuronal and cardiomyocyte circuits (Obien et al. 2014; Fekete 2015; Seymour et al. 2017). The core technology and concepts of contemporary MEA goes back half a century to the pioneering studies of Wise et al. (1970) and Thomas et al. (1972). Whereas great progress has been made over the last 50 years in realizing sophisticated MEA platforms made up of thousands of addressable, high-density, small-diameter low impedance sensors (Berdondini et al. 2005, 2009a, b; Amin et al. 2016; Jackel et al. 2017; Jun et al. 2017; Viswam et al. 2017), the quality of the interfaces formed between the excitable cells (neurons and muscles) and the planar electrodes still remains the weakest constituent of the bioelectronics hybrid. MEA devices based on planar electrodes are "blind" to subthreshold excitatory, inhibitory, and electrotonic synaptic potentials generated by individual neurons. Thus, rather than directly recording and analyzing dynamic changes in synaptic transmission in relation to drugs and toxin screening, different forms of plasticity (learning and memory), or various types of diseases, planar MEA users rely on indirect and complex parameters such as the averages of field potential (FP) frequencies, firing patterns, and others to extract information about the underlying basic biophysical mechanisms. These essentially descriptive FP-related parameters cannot be used to unequivocally analyze and determine diverse synaptic mechanisms or the membrane's excitable properties that underlie the actions of pharmacological reagents, plasticity, or disease pathologies. Crucially, neurons that do not fire action potentials (APs) are not "visible" to planar electrodes and thus go undetected. Since in some

brain areas and possibly in cultures that preserve intact brain properties a fraction of the neurons do not fire or fire at low rates, their proven subthreshold contributions to neuronal computations goes undetected and ignored (Shoham et al. 2006; Epsztein et al. 2011; Barth and Poulet 2012). Ignoring silent neurons due to the technical limitations of cells/planar-electrodes-based MEA goes on despite the documentation that meaningful subthreshold computations play critical roles in neuronal network functions (Lefler et al. 2014).

The enormous advances made over the last 50 years in materials science, microelectronics, and nanoelectronics, together with the acknowledgment of the limitations of substrate-integrated planar MEA, have prompted a number of laboratories to begin merging the advantages of planar MEA technologies (non-damaging and durable) with those of sharp and patch microelectrodes for intracellular recordings of the entire signaling spectrum of neuronal and cardiomyocyte networks. As in the case of research using planar electrode MEAs, the now decade-old generation of nanoelectrode-based MEAs uses passive or active (transistorized) electrodes. However, unlike extracellular planar electrode based MEAs, three-dimensional (3D) vertical nanoelectrodes are designed to perforate or actually penetrate the plasma membrane of cultured cells and thereby form direct Ohmic contact with the cell cytosol. As explained below, when successful, these devices operate in a similar manner to classical sharp-intracellular glass microelectrodes or whole-cell patch electrodes. Because the diameter of 3D vertical nanoelectrodes is in the range of 50–500 nm, penetration of cells by vertical nanoelectrodes was assumed not to damage the plasma membrane or the cells in any significant manner. Although only approximately 10 years has elapsed since the development of the first vertical 3D nanoelectrodes-based MEAs this "young" technology has progressed sufficiently to enable recordings of attenuated intracellular APs and synaptic potentials from neurons, cardiomyocytes, and striated myotubes (Spira et al. 2007; Hai et al. 2010a, b; Tian et al. 2010; Angle and Schaefer 2012; Duan et al. 2012; Fendyur and Spira 2012; Gao et al. 2012; Robinson et al. 2012; Xie et al. 2012; Spira and Hai 2013; Angle et al. 2014; Lin and Cui 2014; Lin et al. 2014; Qing et al. 2014; Rabieh et al. 2016; Shmoel et al. 2016; Abbott et al. 2017, 2018; Dipalo et al. 2017; Liu et al. 2017). Nevertheless, cumulative experience has also pointed to a number of difficulties that require creative solutions. Furthermore, alongside the progress made in intracellular recordings by vertical nanorods, pillars, wires, tubes, and cylinders a recent study emanating from the laboratory of Hongkun Park (Abbott et al. 2017, 2018) confirmed the scaling advantages of nanochip/microchip fabrication technologies by simultaneously recording intracellular APs from hundreds of cultured primary cardiomyocytes, thus heralding a new milestone in MEA technology.

The remainder of this chapter is organized as follows. It begins by familiarizing the reader with the terminology used by briefly describing the cell–electrode interface formed in cultures and presenting a simplified analog electrical circuit depicting the relationships between the two. Next it explains the contribution of the various parameters to the mode of electrical coupling formed between excitable cells and the recording electrode (extracellular or intracellular). This is followed by an examination of the mechanisms that underlie the sealing of the interfacing

junction formed between cultured cells and vertical nanoelectrodes. The next section discusses the mechanisms by which vertical nanoelectrodes make direct Ohmic contact with the cytosol. Multisite, long-term recordings from cultured excitable cells are among the major aims of this novel technology that are yet to be achieved. Thus, it next discusses how conserved cell-biological membrane repair mechanisms that have evolved to protect cells from injury in fact interfere with the presence of nanoelectrodes and curtail the length of time intracellular access can be maintained. Alternative ways of making Ohmic contact between nanoelectrodes and the cell interior that are better able to achieve long-term stability are then considered. The final section presents the earliest and today's cutting-edge achievements of this young technology at the single-cell and network levels. Since different laboratories are currently using different designs, diverse fabrication approaches and materials, the reader is referred to the original publications for technical details. Likewise, different laboratories use different terms to better describe the features of the vertical nanoelectrodes that they have fabricated (pillars, rods, wires, tubes, cylinders, and mushroom-shaped). For the sake of simplicity, we refer in the following to all shapes and forms as vertical nanoelectrodes.

2 The Biophysical Principles that Enable Cell-Noninvasive Extracellular Electrodes to Record Intracellular Potentials

The mode of recordings (i.e., extracellular or intracellular), the quality of the recorded potentials in terms of the signal-to-noise ratio, and electrical coupling (the ratio of the recorded potential to the voltage generated across the plasma membrane V_{elect}/V_{cell}) are defined by three parameters: (a) the electrical properties of the cell's plasma membrane that faces the electrode (the junctional membrane), (b) the seal resistance formed by the gap between the living cell membrane and the electrode surface, and (c) the impedance of the sensing pad and stray capacitance introduced by the conducting lines and the recording amplifier. A simplified analog electrical circuit that depicts these elements superimposed on a schematic drawing of an excitable cell adhering to a 3D microelectrode electrode is illustrated in Fig. 1a. It should be noted that in principle the shown analog circuits represent both 3D and planar electrode–cell interfacings. In this simplified model, the cell's surface area is subdivided into a non-junctional membrane (R_{njm}) that faces the grounded culture medium and a junctional membrane (R_{jm}) that interface with the electrode. Each of these membranes is represented in the circuit by passive electrical elements, a resistor and a capacitor in parallel R_{njm}, C_{njm}, R_{jm}, and C_{jm} respectively. For the sake of simplicity, the circuit and the ensuing analysis ignore the presence of voltage-gated ion channels in the junctional membrane and the anticipated transient changes (increased potassium and decreased sodium and calcium) in the ionic composition of the solution in the restricted volume of the gap between the electrode and the junctional membrane during neuronal activity.

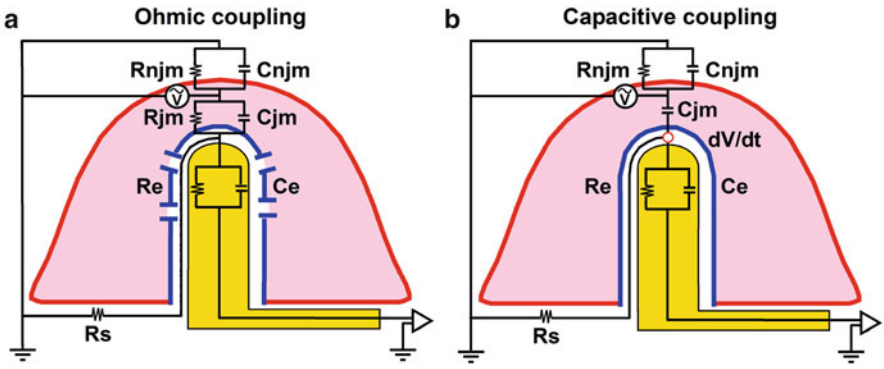

Fig. 1 A schema depicting the basic relationships between a cell (Pink) and a vertical nano-electrode/microelectrode (Yellow) superimposed on a simplified analog electrical circuit. The neuron's plasma membrane is subdivided into a non-junctional membrane (njm, red) that faces the culture medium, and a junctional membrane (jm, blue) that faces the electrode (For details see text). (**a**) When the value of the junctional membrane resistance is low (as indicated by the discontinuous blue line) the electrical coupling coefficient between the cell and the electrode is Ohmic. Under these conditions attenuated spikes and subthreshold synaptic potentials with genuine intracellular features can be recorded. (**b**) When the junctional membrane resistance is high, it can be neglected and the electrical coupling between the neuron and the electrode is capacitive. Under these conditions attenuated signals are recorded as the time derivative of the intracellular electrophysiological signals

The cleft between the cell and the electrode (analogous to the extracellular space between living cells in tissue) is represented by a single resistor (R_s). The value of R_s is defined by the dimensions of the contact area between the cell's membrane and the sensing electrode. The electrode is represented by a resistor and capacitor in parallel (R_e and C_e respectively).

Changing the relationships between the junctional membrane properties, the seal resistance, and the electrode impedance is expected to robustly alter the recording mode from extracellular to intracellular, and change the shape and the amplitude of the recorded potentials from microvolts to tens of millivolts. A quantitative estimate of the expected electrical coupling levels between a given excitable cell and a particular microelectrode configuration can be acquired by the use of various analog electrical circuit simulators (e.g., the open source SPICE). The values of the electrical elements comprising a given analog circuit and the input voltage (spike or synaptic potential) can be experimentally extracted or estimated. Various approaches to obtain and estimate the parameters of a given cell–circuit hybrid and the simulation outcomes will not be described here. For examples the reader is referred to the following publications: Fromherz (2003), Hai et al. (2010a, b), Fendyur et al. (2011), Sileo et al. (2013), Spira and Hai (2013), Angle et al. (2015), Massobrio et al. (2016), Shmoel et al. (2016), Dipalo et al. (2017), Abbott et al. (2018), and Massobrio et al. (2018).

Remarkable experimental manipulations supporting the above suppositions were provided almost 20 years ago by Jenkner and Fromherz (1997) using isolated leech neurons, and later by Cohen et al. (2008) using *Aplysia* neurons. In both studies a sharp recording and stimulating intracellular electrode was inserted into a neuron's somata cultured on a substrate-integrated flat electrode (Fig. 2). In addition, a micromanipulator-driven fire-polished pipette positioned on top of the neuron was used to displace the cell body or its thick axon towards the planar electrode and

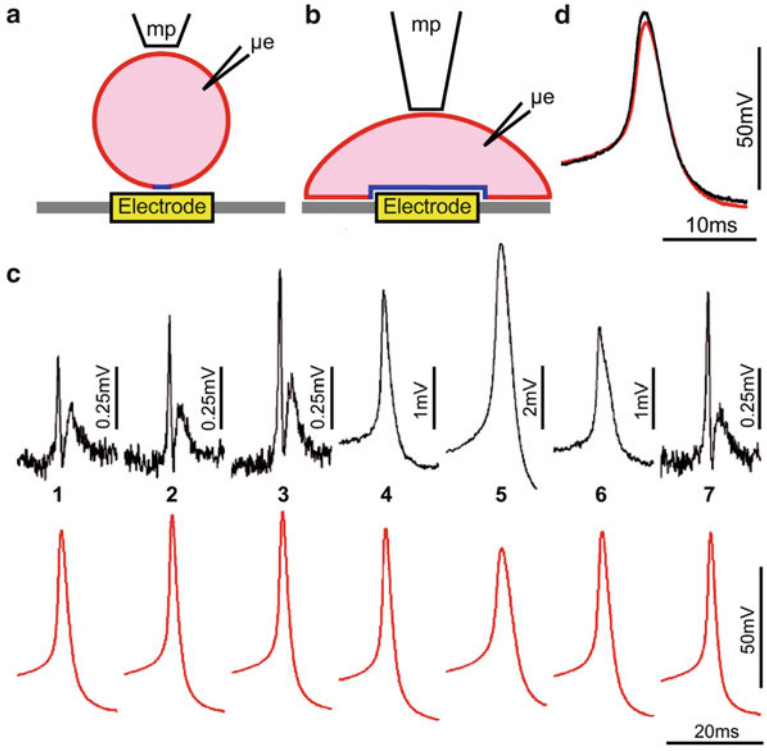

Fig. 2 From extracellular to intracellular recordings by compression of a neuron onto the surface of a substrate-integrated planar electrode. (**a**) A schema depicting a cultured Aplysia neuron cell body residing on the surface of a planar electrode. A fire-polished glass micropipette (mp) compress the cell body downwards towards the flat electrode (yellow) (**b**), while recording the transmembrane potential by an intracellular sharp electrode (µe). (**c**) Intracellular voltage recordings in red and extracellular field potential recordings by the planar electrode in black. Initially as the cell was compressed downwards (*c1* to *c3*) the amplitude of the FP increased while the intracellularly recorded AP maintained its amplitude. Further increase in the applied pressure lead to transition of the recorded action potential from extracellular to intracellular (*c3* to *c4*). This was accompanied by a decrease in the amplitude of the intracellularly recorded AP (red traces *c4* and 5). Releasing the pressure (*c6* and *c7*), lead to reversal of the process. Note the differences in the vertical scale bars along the black traces. (**d**) Overlapping of the normalized potentials recorded by the sharp and flat electrodes (*c5*) (Reprinted with permission from Cohen et al. (2008). Copyright Elsevier Biosensors and Bioelectronics 2008)

its surrounding substrate (Fig. 2). Gentle downward compression of the cell by the fire-polished pipette concomitant with readjustment of the intracellular electrode position was done under visual control. Both Jenkner and Fromherz (1997) and Cohen et al. (2008) reported that when the somata or an axon was mechanically displaced downwards towards the surface of a planar electrode, the contact area between the cell and the substrate increased (Fig. 2). This gradual increase in the contact area was accompanied by an increase in the amplitude of the FP generated by a depolarizing pulse delivered to the neuronal cell by the sharp intracellular electrode. The increased FP amplitude was not associated with a significant change in the FP shape (Fig. 2). Concomitant intracellular recordings of the APs by the sharp glass electrode revealed that the intracellular spike amplitude and shape were not altered. The increased amplitude of the extracellular FP was attributed to increased R_s due to the increased contact area between the neuron and the electrode, and possibly also due to reduction in the cleft width (Fig. 2). Further increase in the mechanical pressure transformed the extracellular FP (recorded by the planar electrode) into positive monophasic attenuated APs with the characteristic shapes of classical intracellular recordings (Fig. 2). It is important to note that the transition between extracellular FP to an attenuated intracellular AP was accompanied by the decreased amplitude of the intracellularly recorded AP by the sharp electrode. This indicated that stretching the neuron's plasma membrane against the substrate led in addition to the increased Rs to a transition of the cell–electrode coupling from capacitive to Ohmic, probably by generating nano-holes along the stretched membrane that faced the planar electrode. Releasing the mechanical pressure led to a reversal of all the parameters, including the contact area, the FP recorded by the planar electrode, and the amplitude of the intracellularly recorded AP (Fig. 2). These experiments thus demonstrated the potential to alter the recording mode from extracellular to intracellular by reducing the junctional membrane resistance and increasing the seal resistance.

3 Formation of Seal Resistance

The formation of high seal resistance between a cultured cell and an electrode requires the optimal positioning of the cells with respect to the electrode. Unfortunately, initial cell–electrode contact is a low-probability event driven by the gravity of the seeded cells. Currently, the most practical way to increase the likelihood of optimally positioning cells in contact with electrode is by increasing the cells' seeding density and/or the density of the electrodes. Once cells form physical contact with the substrate of the device, they adhere to it by chemophysical process and chemical recognition events of molecular entities anchored to the substrate and receptors in the outer leaflet of the plasma membrane (Sackmann and Bruinsma 2002). The value of seal resistance formed under these conditions is defined by the planar dimensions of the cell-sensing pad junction and the width of the cleft formed between the plasma membrane and the electrode surface (Weis and Fromherz

1997). Using optical methods and biophysical analysis, Braun and Fromherz (1998) and Zeck and Fromherz (2003) estimated that the cleft width formed between rat astrocytes cultured on silicon dioxide coated by laminin was approximately 100 nm. Accordingly, the R_s was estimated to be in the range of single MΩs (Weis and Fromherz 1997). Electron microscopic analysis of thin sections prepared from cultured *Aplysia* neurons grown on 2D-polyaniline-coated glass substrate revealed that the cleft width ranged from hundreds of nanometers in some areas to 20–40 nm in others (Oren et al. 2004). There is a general consensus that cleft dimensions of approximately 20 nm correspond to the minimum width that can be formed by cells grown on substrates coated with biocompatible molecules (Sackmann and Bruinsma 2002). Although the seal resistance, which is in the range of a single MΩ, suffices to enable recordings of extracellular FPs, it is insufficient to enable intracellular recordings. Theoretically, increasing the planar dimensions of the gap between the junctional membrane and the electrode surface should increase the seal resistance (as shown in Fig. 2). However, this cannot be applied to small neurons or other cell types and in particular not to cultured cell networks.

Experiments conducted using different forms of 3D vertical nanoelectrodes have revealed that in spite of the small surface area of these nanostructures, the seal resistances formed between cultured cells and the nanostructures have significantly higher values in the range of 50–500 MΩ than those formed by planar electrodes of larger surface areas (single MΩ values) (Hai et al. 2009a; Robinson et al. 2012; Lin et al. 2014; Dipalo et al. 2017). Apparently, independent of the precise geometry of the 3D structure but limited by the dimensions and pitch (Hanson et al. 2012; Ojovan et al. 2015) the seal resistance around vertical nanostructures is generated by cell-biological mechanisms that actively "engulf" 3D vertical nanostructures (Fig. 3a, b) yielding almost an order of magnitude larger seal resistances than that observed for planar electrodes. This process is apparently associated with a reorganization of the submembrane skeleton and membrane proteins along the junctional membrane. For example, using live confocal microscope imaging, Hai et al. (2009b) documented the formation of actin rings around the stalk of gold mushroom-shaped microelectrodes when cultured Aplysia neurons are interfaced with 3D microelectrodes (Fig. 3c).

The structural analysis of chemically fixed junctions formed between cells and nano/micro vertical electrodes by transmission electron microscopy (Spira et al. 2007; Hai et al. 2009a, b, 2010a, b; Hanson et al. 2012) and focused ion beam microscopy (Santoro et al. 2017) revealed that whereas cells tightly engulf the vertical nanostructures, these nanostructures do not spontaneously penetrate the cell's plasma membrane. This structural observation is consistent with electrophysiological observations indicating that in most cases unless the vertical nanoelectrodes are "forced" to perforate or fully penetrate the plasma membrane by electroporating pulses they maintain their extracellular position. Apparently, this conclusion is contradicted by studies demonstrating the transfer of molecules that adhered to the surface of nanopillars to cells residing on them. Nevertheless, it was noted that the probability of spontaneous transfer of optically labeled molecules is low (Xu et al. 2014).

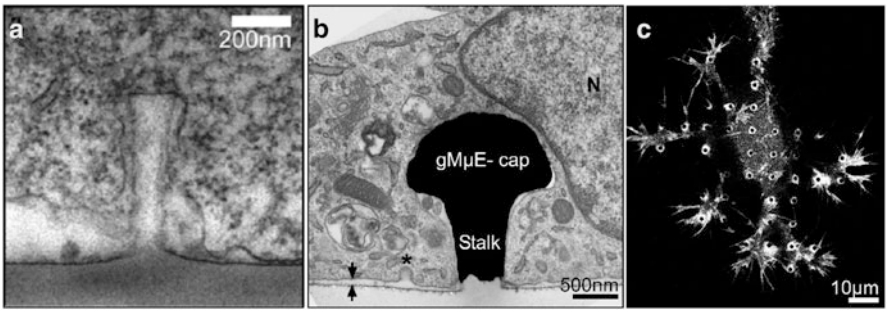

Fig. 3 Electron microscope images of a vertical nanopillar (**a**, Reprinted with permission from Hanson et al. (2012). Copyright American Chemical society Nano Letters 2012) and a gold mushroom-shaped microelectrode (**b**, Reprinted with permission from Hai et al. (2010a) Copyright Nature Publishing Group 2010) engulfed by LH-1 cell and a PC12 cell. Note that the cell's membrane tightly engulfs the vertical nanoelectrode. (**c**) Confocal microscope images of actin rings formed by cultured Aplysia neuron around the stalk of a gold mushroom-shaped microelectrode

Taken together, although the seal resistance formed between cultured cells and vertical nanostructures is (50–500 MΩ) roughly an order of magnitude larger than the one formed between cultured cells and planar electrodes, it is still far from the GΩ seal values formed by classical patch electrodes and plasma membranes.

Because successful intracellular recordings by vertical nanoelectrodes depend on the parallel formation of high seal resistance and low junctional membrane resistance, the next paragraph discusses potential mechanisms to concomitantly increase both parameters.

4 The Reduction of the Junctional Membrane Resistance Is a Critical Parameter to Gain Effective and Durable Intracellular Access

Gaining direct access to the cell cytosol by "piercing" the plasma membrane with a sharp glass microelectrode or by mechanically "breaking" the plasma membrane by suction through a patch electrode along with the formation of a GΩ seal resistance between the glass wall of the electrodes and the plasma membrane (Fig. 4) enables genuine intracellular recordings which can last from minutes to hours (Sakmann and Neher 1984). As the solution contained within the patch electrode gradually perfuses into the cytosol, it alters its ionic content and dilutes diffusible molecular entities of the cytosol. With time, this process interferes with the normal physiology of the cells. To overcome this problem Horn and Marty (1988) developed the perforated patch configuration. Rather than breaking the cell's membrane to gain Ohmic access to the cytosol they introduced ionic channels such as nystatin or gramicidin into the patch electrode solution. These channels then integrate with the plasma membrane

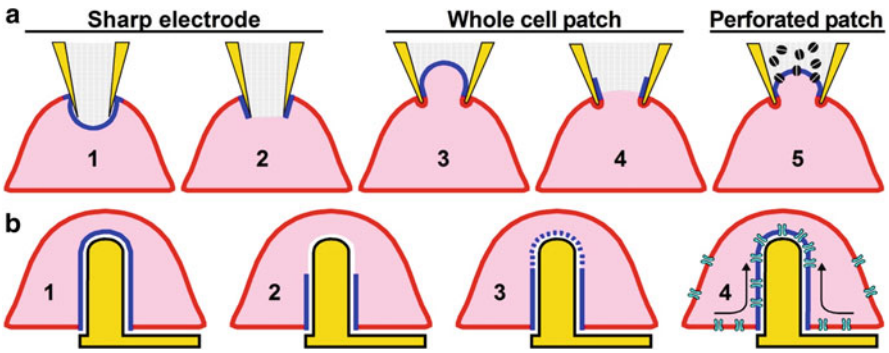

Fig. 4 Schema depicting cell–electrode interfacings formed by classical intracellular electrodes (**a**), and vertical nanoelectrodes (**b**). When a sharp glass microelectrode is mechanically driven against the cell membrane it forms a "membrane dimple" (*a1*, blue). An electroporating pulse breaks open the plasma membrane that faces the electrode tip and a seal is formed between the external side of the glass wall and the cell plasma membrane (*a2*). In the whole-cell patch configuration a membrane patch is sucked into the electrode (*a3* blue). Application of additional suction breaks the membrane open and a GΩ seal is formed between the plasma membrane and the inner surface of the glass wall (*a4*). A similar configuration (to *a1* and *a3*) is formed between a cell that engulfs a vertical nanoelectrode (*b1*). Under these conditions when an electroporating pulse is delivered through the nanoelectrode (*b2* or *b3*), the junctional membrane (blue) is either pierced (*b2*) or porated (*b3*). Another electrode/cell recording configuration is the whole-cell perforated patch (*a5*) in which after GΩ seal formation ion channels within the patch electrode (black) integrate with the plasma membrane to lower the junctional membrane resistance (*a5*). A similar configuration might be formed around an engulfed vertical nanoelectrode by recruiting of ion channels into the junctional membrane around the vertical nanoelectrode (*b4*)

to reduce its resistance (Fig. 4). Together with the formation of high seal resistance between the plasma membrane and the internal wall of the patch pipette, a perforated GΩ patch configuration is formed (Fig. 4a-5). Note that in the perforated patch configuration, the electrode remains outside of the cell but records intracellular potentials, whereas in the case of sharp electrodes and the whole-cell configuration the electrode tips are practically in the cytosol (Fig. 4a-2 and a-4).

Intracellular recordings by vertical nanoelectrodes are based on the same principle of gaining low resistance access to the cytoplasm.

Local membrane poration by current pulses delivered by vertical nanoelectrodes have proven to be the most useful approach to lower the junctional membrane resistance (Braeken et al. 2012; Hai and Spira 2012; Robinson et al. 2012; Xie et al. 2012; Lin et al. 2014; Abbott et al. 2017, 2018). In fact, it still remains unclear whether after electroporation the tip of the nanoelectrodes pierces the plasma membrane (Fig. 4b-2) or generates nanoholes in the junctional membrane (Fig. 4b-3). Whatever the actual mechanism, intracellular access by electroporation is transient and only lasts minutes to approximately 1 h. Thereafter, the electrodes are insulated from the cytosol (Hai and Spira 2012; Xie et al. 2012; Lin et al. 2014; Abbott et al. 2017; Dipalo et al. 2017). The electrode insulation process is

most likely generated by conserved membrane repair mechanisms. A study of the cascades underlying electrical insulation of an electrode after electroporation (Hai and Spira 2012) showed that focal membrane electroporation by gold mushroom-shaped microelectrodes leads to localized increases in the free intracellular calcium concentration ($[Ca^{2+}]_i$) around the electroporating electrode along with a concomitant reduction in the cell's input resistance (R_{in}). This is probably due to reduction in the seal and junctional membrane resistances. Thereafter, within minutes, the input resistance of the cell recovers along with the recovery of the $[Ca^{2+}]_i$. Membrane repair mechanism after injury is a highly conserved cell biological mechanism that serves cells in general and muscle fibers in particular to withstand a variety of physiological and pathological membrane disruptions. Likewise, most cell types, including in particular muscle fibers and neurons, have evolved efficient calcium removal mechanisms. Current concepts suggest that localized membrane repair is triggered by the influx of calcium ions into the cytosol across the large extracellular/intracellular calcium concentration gradient and possibly by the release of calcium ions from intracellular stores. The elevated $[Ca^{2+}]_i$ induces exocytosis of intracellular vesicles such as lysosomes that leads to the formation of "membrane patches" that seal the "punctured" plasma membrane (Fig. 5) (McNeil and Khakee 1992; McNeil and Kirchhausen 2005; Han and Campbell 2007). A complementary mechanism could also be lateral recruitment of membrane into the injured patch (Demonbreun and McNally 2016). The findings of Hai and Spira (2012) were consistent with the "membrane patching model" in that the dynamics of the recovery process from electroporation progressed in discrete steps. It is conceivable that the effective calcium removal mechanisms of cultured neurons and cardiomyocytes enabled the cells to withstand repeated electroporations over a number of days, as reported in a number of studies (Fendyur and Spira 2012; Robinson et al. 2012; Lin et al. 2014; Rabieh et al. 2016; Dipalo et al. 2017). Since there is ample evidence that

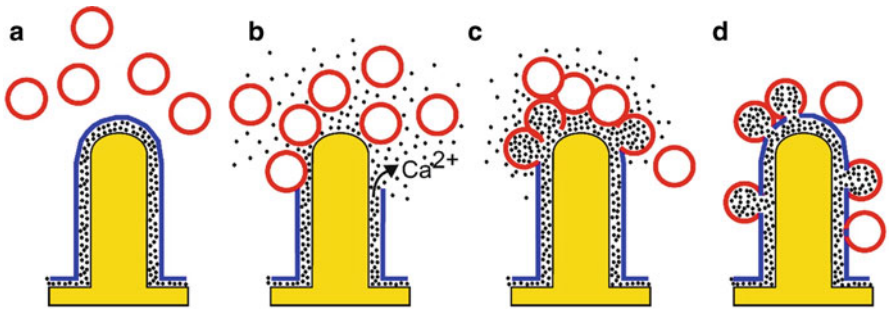

Fig. 5 Schematic representation of the membrane "patch repair" mechanisms. Injury of the plasma membrane (from **a** to **b**) leads to calcium ions influx (black dots) into the cell. The elevated free intracellular calcium ion concentration leads to fusion of intracellular vesicles with the injured patch of the membrane (**c**). (**b**, **c**) Depicts a hypothetical case of membrane piercing by the vertical nanoelectrode. (**d**) Once the membrane is repaired the free intracellular calcium concentration is downregulated to the control level

membrane repair mechanisms are ineffective in patching large diameter holes (Joshi and Schoenbach 2002), it is paradoxically possible that the nanometric dimensions of the electrodes which facilitate their penetration through the plasma membrane underlie the relatively fast process of insulation.

In an attempt to improve the "insertion" of vertical nanoelectrodes into cells, the work by the Francesco De Angelis laboratory (Dipalo et al. 2017) has used plasmonic optoporation to porate the junctional membrane (Messina et al. 2015). They reported that cultured neurons and HL-1 cells can be seamlessly plasmonically optoporated without interrupting ongoing spontaneous action potential activity. Nonetheless, even under these advantageous conditions, intracellular recordings were limited to just over an hour, at which point the electrodes were insulated.

In view of the above observations and the understanding that robust cell biological process underlie it, future approaches to stabilizing nanoelectrode–cytosol contact could attempt to prevent the initiation of membrane repair cascades by limiting the calcium influx (or its release from intracellular stores) or by transiently increasing the calcium buffering capacity of the cells. This is possible by functionalizing vertical nanopillars with molecular entities that effectively fuse and integrate the electrode surface with the plasma membrane (Chernomordik and Kozlov 2008). This approach was developed and tested by the N. Melosh laboratory (Almquist and Melosh 2010, 2011; Verma et al. 2010; Almquist et al. 2011) which was then replicated as proof of concept by a number of laboratories. Recently, VanDersal and Renaud (2016) used cultured DHHC6-depleted HeLa cells (that spread over surface areas better than conventional HeLa cells) to adhere to a planar electrode which resided within a 5 nm thick gold ring decorated by 5 nm thick self-assembled alkanethiol chains. As the HeLa cells spread over the rings, the alkanethiol chains spontaneously fuse with the outer leaflet of the plasma membrane, generating a seal resistance around the planar electrode in the range of 5 GΩ, thus generating a cell attached patch configuration without resorting to suction (Fig. 6). The application of a brief electroporating pulse by the electrode residing within the gold ring transformed the cell attached configuration into a whole-cell patch configuration. Note that under these conditions, the cytosol is not perfused and the whole-cell patch configuration can remain effective for up to 72 h,

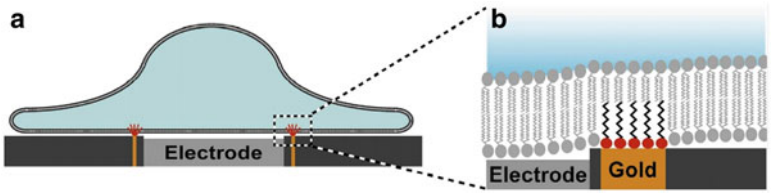

Fig. 6 A schema depicting spontaneous GΩ seal formation when a cultured cell (blue) extends over a substrate-integrated gold ring (yellow) functionalized by alkanethiol (red) encompassing a planar electrode (gray). (**a**) Cross section of a cell adhering to the substrate and the 5 nm thick gold ring functionalized by alkanethiol. (**b**) Enlargement of (**a**) (Reprinted with permission from VanDersal and Renaud (2016). Copyright Sci Rep 2016)

which is significantly longer than any other study attempting to generate a durable low resistance junction between cultured cells and the electrode. As anticipated by the N. Melosh laboratory when adapted to vertical nanopillars, an effective GΩ seal could be formed and therefore reduce, if not prevent, calcium influx after electroporation and hence avoid triggering membrane repair mechanisms and electrode insulation.

Besides electroporation and plasmonic optoporation, increased junctional membrane conductance may be induced by the recruitment of ion channels into the junctional membrane (Fig. 4b-4). Two mechanisms have been considered. Hai et al. (2010a) suggested that culturing *Aplysia* neurons in contact with gold mushroom-shaped microelectrodes functionalized by a multiple Arg-Gly-Asp (RGD) repeat peptide could facilitate the physical contact between the plasma membrane and the electrodes and that the binding of the peptide to receptors on the plasma membrane could lead to structural reorganization of the submembrane skeleton. This in turn might be followed by changes in the density and possibly the type of ionic channels at the junctional membrane. Interestingly, the recruitment of a relatively small number of such channels would suffice to elevate the junctional membrane conductance to support effective electrical coupling. For example, assuming that the junctional membrane conductance (of cultured *Aplysia* neurons) is increased by recruitment of voltage-independent potassium channels with a channel conductance of 10 to 100 pS, 10–100 channels would need to be concentrated within a confined junctional membrane area of 14 μm^2 to reduce the junctional membrane resistance from an estimated value of 100 GΩ to 100 MΩ. This would imply a channel density of 0.5 to 10 channels/μm^2 (Hai et al. 2010a). Interestingly, this type of potassium channel density has been experimentally documented in a number of cell types (Hille 1992).

An alternative mechanism that could lead to accumulation of ion channels within the junctional membrane is the imposed curving of the plasma membrane around the vertical nanoelectrodes. Membrane curvatures have been shown to trigger molecular cascades that could underlie local changes in the expression and density of membrane proteins including ion channels (Epand et al. 2015; Iversen et al. 2015; Lou et al. 2018). In recent studies by the laboratory of B Cui, Zhao et al. (2017) and Lou et al. (2018) documented increased profiles of clathrin-coated pits and the accumulation of clathrin and dynamin at the junctional membrane of SK-MEL-2 cells. This indicated that clathrin-mediated endocytosis is enhanced by the membrane curvature induced by the nanopillar tips. The cytoskeletal element actin was also shown to concentrate around curved membranes (Hai et al. 2009b, and Fig. 3) because actin and its associated proteins are involved in diverse cellular functions; these results may suggest that membrane curvature might affect among other cellular processes the recruitment of ion channels.

5 Reading the Electrophysiological Signaling Repertoire Recorded by Various Types of 3D Nanostructures and Microstructures

The overarching purpose of developing intracellular recording MEA is to produce easy-to-use devices that not only improve the source resolution of AP but can monitor online (without averaging) the entire electrophysiological signaling repertoire of neuronal and cardiomyocyte networks. One characteristic shared by all newly developing technologies is that different investigators experiment with different approaches, designs, materials, and fabrication processes. As a result, identical source signals may be modified in different ways by different recording devices. The quality of electrophysiological recordings may thus range from genuine intracellular recordings of APs and synaptic potentials to complex recordings of integrated extracellular and intracellular potentials or from time derivatives of intracellular recordings as in loose seal configurations (juxtacellular recordings) to classical intracellular APs (Joshi and Hawken 2006; Gold et al. 2009). The next section discusses a few examples and illustrates the relationships between the principles of device and interface designs and the ensuing signal readout. As different laboratories use different fabrication approaches and materials, the reader is referred to the original publications for detailed information on this aspect.

6 Optimal Intracellular Recordings by Scalable Field Effect Transistor Technology

Early in the evolution of scalable 3D nanoelectrodes for intracellular recordings the CM Lieber laboratory pioneered the development and use of a nano-field-effect transistor (FET) located at the tip of a "kinked nanowire" (Tian et al. 2010). Since the performance of FETs does not depend on the impedance between the chemically functionalized nano-FET and the cell, Tian et al. (2010) were able to record endogenously generated APs with amplitudes and shapes identical to intracellular recordings by patch electrodes from single cells.

The initial FET approach that was designed to record from single cells was soon improved by synthetically integrating SiO_2 nanotube on top of the nanoscale FETs. The insertion of lipid-coated SiO_2 FETs nanotube into the cell brought the cytosol into Ohmic contact with the FET and enabled recordings of full-blown transmembrane potentials (Fig. 7a) (Duan et al. 2012). To the best of our knowledge there have been no further applications of the nano-FET located at the tip of a "kinked nanowire" for simultaneous recordings from many individual neurons or cardiomyocytes within a given in vitro network. Recently, the laboratory of H. Park (Abbott et al. 2017) successfully scaled up transistorized vertical nano-MEA device to simultaneously record attenuated intracellular APs from a network of a few hundred cardiomyocytes.

7 Attenuated Intracellular Recordings of Action Potentials by Passive Nanoelectrodes After Membrane Poration

Along with advances in the technology of nanoscale FET electrodes, passive vertical nanowires, pillars, and tubes-based MEA were developed and tested. The Bianxiao Cui laboratory (Xie et al. 2012) fabricated vertical Pt nanowire electrodes (150 nm in diameter and 1–2 μm in height) to simultaneously record endogenous activity from a number of cultured HL-1 cells (Claycomb et al. 1998). Each recording unit was constructed from a common 5 × 5 μm^2 insulated pad from which five vertical nanowires protruded (Fig 7b). Electroporation transformed the extracellularly recorded biphasic FPs by the vertical nanowires to an intracellular recording mode whose shape resembled APs recorded by whole-cell patch electrodes with attenuated amplitude of 1–10 mV (Fig. 7b). Conceivably membrane repair mechanisms caused the porated junctional membrane to gradually recover along with an unavoidable decrease in the AP amplitude and finally the reversal of the recording mode from intracellular to extracellular within 10 min. Electroporation of the same cell could be repeated over a number of days, suggesting that the cells fully recovered from the trauma of electroporation. By using iridium oxide (IrOx) nanotubes rather than solid Pt wires, the Cui laboratory (Lin et al. 2014) caused cultured HL-1 cells and primary rat cardiomyocytes not only to enwrap the vertical tube but also to protrude into its hollow center. The tight interface resulted in recording larger APs (in the range of 1.5–15 mV) for longer durations ranging from minutes to an hour after the delivery of an electroporating pulse. The slow reversal process under these conditions gave sufficient time to examine characteristic pharmacological effects of specific drugs on the frequency and shape of the spontaneous APs. Furthermore, repeated intracellular recording by electroporation could be conducted for 8 days.

In the same year (2012) the Hongkun Park laboratory undertook the challenge to interface scalable vertical nanowires based MEA with cultured mammalian neurons for the first time (Robinson et al. 2012). It should be emphasized that primary cardiomyocytes and in particular the LH-1 cell line cultured on MEA cannot be used as models to predict the recording quality from primary neurons. This is mainly due to the fact that LH-1 cells and cardiomyocytes spread radially over a large surface area, adhere well to the substrate and therefore form high seal resistance around the electrodes. In contrast, cell bodies of mammalian neurons are small, do not spread and adhere as well as cardiomyocytes and thus form lower seal resistances.

Using recording units constructed of nine Ti/Au metallic tips vertical nanowires (150 nm diameter, 3 μm height) the Hongkun Park laboratory (Robinson et al. 2012) recorded intracellular APs of ∼4 mV and were able to stimulate selected cortical neurons to fire action potentials (Fig. 7c). To gain intracellular access for recordings and stimulation, the junctional membrane was electroporated. Although the recordings were of high amplitude, no indications of synaptic communication among the neurons were documented by the vertical nanoelectrodes.

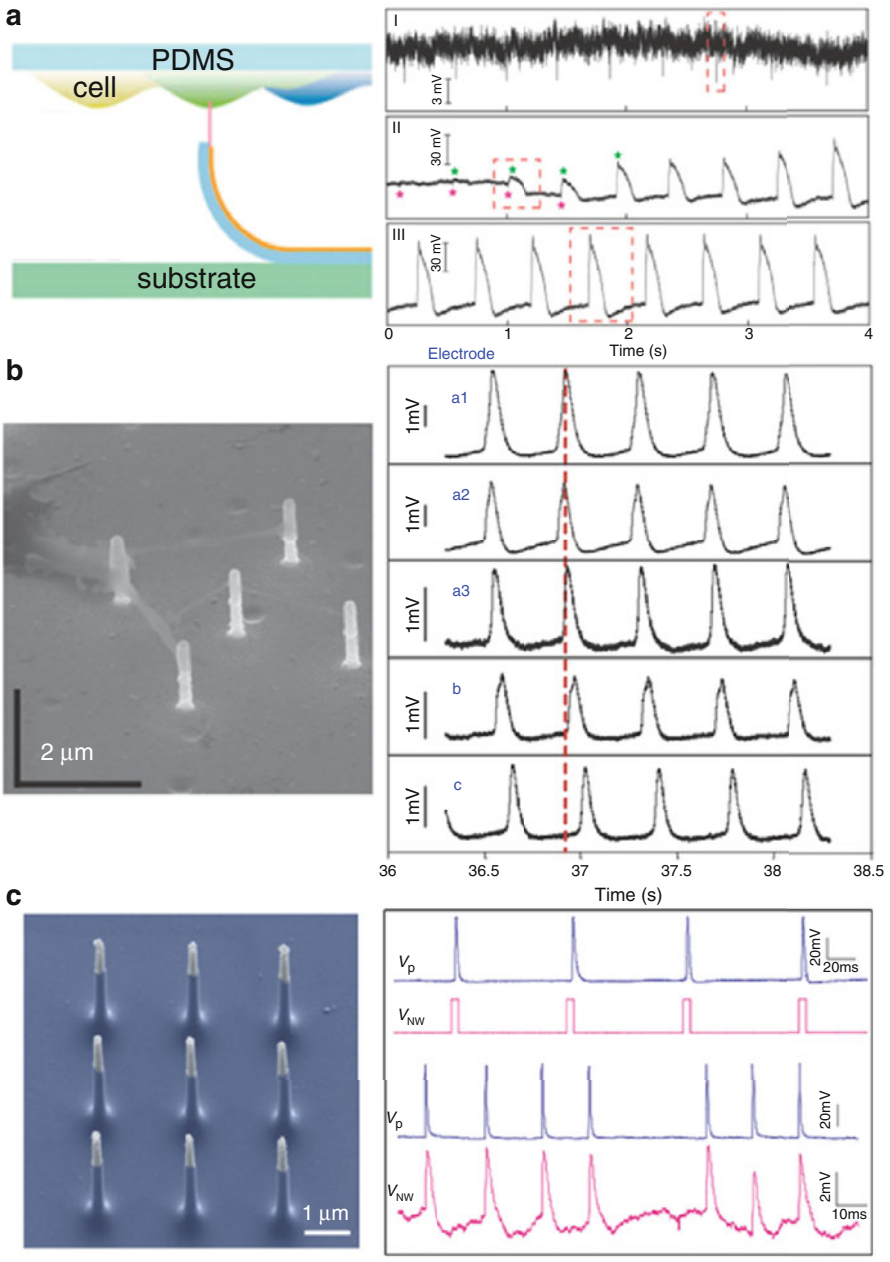

Fig. 7 Examples of the intracellular recording qualities of vertical nanoelectrode arrays. (**a**) Schematics of 3D kinked nanowire FET probe interfaced with an "upside-down" applied sheet of HL-1 cells grown on a PDMS substrate (left). Before insertion of the FET into a cell (I) extracellular FPs are recorded. Insertion of the nanoelectrode through the plasma membrane is associated by a hyperpolarization shift of the recorded potential and transition of the extracellular

In a recent set of experiments the F. De Angelies laboratory (Dipalo et al. 2017) significantly improved the methods to gain direct contact between vertical nanoelectrode and the cytosol. Dipalo et al. (2017) fabricated vertical 3D gold plasmonic nanocylinders with a diameter of 150 nm and a height of 1.8 μm on planar electrode (21 × 21 μm) that was electrically in contact with the culturing medium (Fig. 8). The metal coating of the nanocylinders was connected to the planar base (De Angelis et al. 2013; Dipalo et al. 2015). Endogenous APs generated by LH-1 cells that adhere to the flat electrodes and substrate around it were recorded as typical extracellular FPs (inward current, Fig. 8). Instead of electroporation pulses aimed at "piercing" the junctional membrane, they developed the plasmonic optoporation approach in which a short laser pulse "open transiently nanopores exclusively at the tip" of the vertical nanopillar (Messina et al. 2015; Zilio et al. 2017). The ability to precisely control the laser beam was used to optoporate single vertical electrode at a time. This gave the authors the unique opportunity to experimentally determine the contribution of each pillar and the planar electrode to the shape and amplitude of the recorded potential (Fig. 8). Plasmonic optoporation of the cell membrane by one nanopillar changed the recorded extracellular potential to a hybrid extracellular–intracellular potential. When two nanopillars were plasmonically optoporated the weight of the intracellular components was more pronounced. Finally, when all four nanopillars were optoporated, the features of the recorded potentials were comparable to intracellular recordings (Fig. 8). Importantly, the "insertion" of the vertical nanoelectrodes by optoporation did not interfere with the endogenous patterns of AP firing by the cells. This indicates that the optoporation pulse used did not induce a large increase in the cell's membrane resistance, nor did it lead to elevated $[Ca^{2+}]_i$. Nevertheless, since the intracellular recordings configuration did not last for more than an hour, it is conceivable to assume that micrometric motion of the cells in respect to the substrate led to the isolation of the electrodes from the cells. Importantly, this study also documented the presence of spontaneous small amplitude potentials (~40 μV) with features reminiscent of synaptic potentials. Although the authors did not argue that these potentials were genuine synaptic potentials, it is reasonable to assume that indeed they are. It should be noted, however, that because the cell bodies of the cultured neurons may not adhere and

Fig. 7 (continued) FPs to full blown 80 mV intracellular APs (II, III) (Reprinted with permission from Tian et al. (2010) Copyright Science, 2010). (**b**) Passive nanopillar electrode-based MEA constructed of five vertical nanoelectrodes on a common platinum pad. Intracellular recordings were simultaneously obtained from five individual HL-1 cells (right) (Reprinted with permission from Xie et al. (2012). Copyright Nature Publishing Group, 2012). (**c**) Vertical nanowire MEA constructed of nine silicon nanowires on a common pad. Shown are bidirectional recordings and stimulations of cultured primary neurons by the vertical nanoelectrodes concomitantly with recording by patch electrodes. Stimuli applied by the vertical nanoelectrode (2nd trace) evoked action potentials recorded by the patch electrode (1st trace). Stimulations delivered by the patch electrode (3rd trace) evoked action potentials recorded by the nanowire electrode (4th trace) (Reprinted with permission from Robinson et al. (2012). Copyright Nature Publishing Group, 2012)

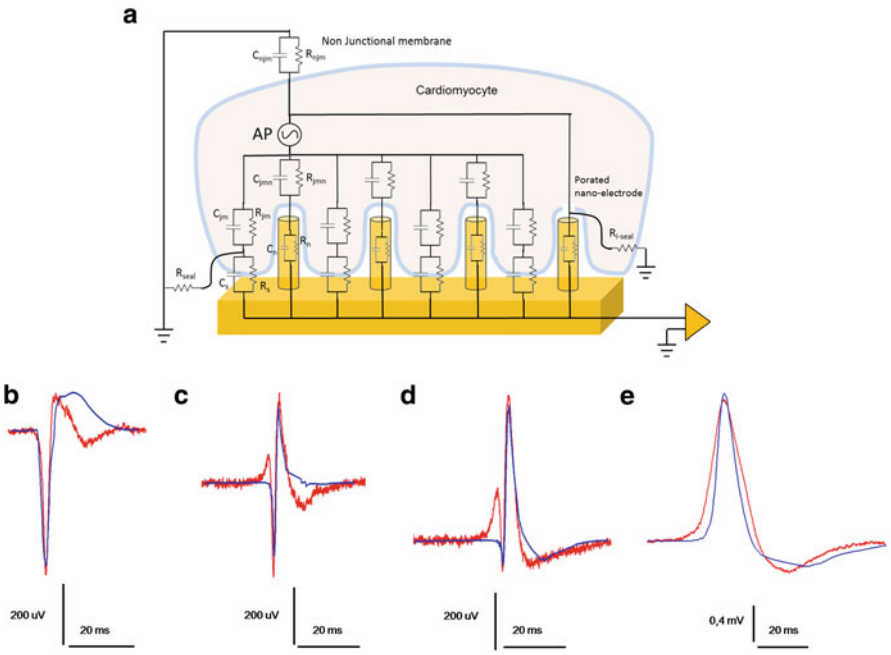

Fig. 8 An analog electrical circuit of a combined planar/vertical nanoelectrodes MEA used to simulate and experimentally study the advantages of plasmonic cell optoporation. (**a**) The analog electrical circuit used to simulate (**b**, blue traces) the actual recordings (**b** red traces). When one or two out of the four vertical nanoelectrodes optoporated the HL-1 cell, the recorded extracellular potential (**b**) transforms to "mixed" extracellular–intracellular recorded potential (**c**, **d**). When all four vertical nanoelectrodes optoporate the cell, the shape of the recorded potentials becomes almost identical to that of genuine attenuated intracellular recordings (**e**) (Reprinted with permission from Dipalo et al. (2017). Copyright ACS https://pubs.acs.org/doi/abs/10.1021%2Facs.nanolett.7b01523. Note: further permissions related to the material excerpted should be directed to the ACS)

cover the entire surface of the flat part of the electrode, it is theoretically possible that these "tentative synaptic potentials" are in fact pickups of FPs generated by remote neurons. If these are genuine synaptic potentials, this together with the report published by the S. Dayeh laboratory (Liu et al. 2017) and work by Shmoel et al. (2016) would be the first to tentatively document recordings of spontaneous synaptic potentials by vertical nanoelectrodes.

Taken together, these results show that at a proof-of-concept level scalable passive vertical nanoelectrodes can be manipulated to form transient contact with the cytosol and have a large enough seal resistance to record attenuated intracellular APs with features similar to whole-cell patch or sharp electrodes. The attenuation of the signals is the outcome of the high impedance of the 3D vertical nanostructures due to their small surface area. Attempts to overcome this limiting factor by the use of multiple vertical nanoelectrodes only partially improve the situation. Another

critical shortcoming of currently used vertical nanoelectrode technology is the limited time (an hour) for intracellular access after membrane electroporation or optoporation. The inhibition or slowdown of the innate membrane repair mechanism which serves to protect cells from damage and isolates the nanoelectrode after membrane poration can be theoretically designed. The issues of high electrode impedance could be overcome by the use of nano-FETs (the CM Lieber solution) and the development of novel materials. The quality of the seal resistance could be substantially improved by developing suitable surface chemistries to effectively fuse the electrodes with the cell membrane (Almquist et al. 2011; Almquist and Melosh 2011; VanDersal and Renaud 2016).

Finally, so far none of the multiple vertical nanoelectrode devices have been effectively applied to monitor the entire electrophysiological repertoire from individual neurons comprising a neuronal network. Nonetheless, the successful scaling of the vertical nano-MEA device by the H. Park laboratory (Abbott et al. 2017) to simultaneously record attenuated intracellular APs from a network of a few hundred cardiomyocytes is a significant achievement marking a new milestone in vertical nanoelectrode array technology.

8 Extracellular Gold Mushroom-Shaped Microelectrode Arrays for Intracellular Recordings

Along with the development of vertical nanoelectrode technologies which in principle operate like classical sharp and whole-cell patch microelectrodes, our laboratory has begun to test a different approach which purposely limited the cell–electrode configuration to a perforated patch electrode arrangement. In contrast to the vertical nanoelectrodes that are designed to penetrate the cells membrane, we used gold mushroom-shaped microelectrodes (gMμEs) with a relatively large cap with a diameter of 1.5–2 μm, a stalk diameter of ∼1 μm, and a height of ∼1.5 μm (Spira et al. 2007, and Fig. 3b). These gMμE record attenuated synaptic and APs from cultured Aplysia neurons with the characteristic features of intracellular recordings by forming a high seal resistance and the induction of low junctional membrane resistance that faces thee electrode (Spira et al. 2007; Hai et al. 2010a, b; Spira and Hai 2013). In these studies, 48–72 h after culturing juvenile *Aplysia* neurons on an RGD repeat functionalized gMμE surface, attenuated APs and subthreshold potentials with characteristic features of intracellular recordings were monitored (Fig. 9). Since the gMμEs are engulfed by the neuron but remain outside of it (Fig. 3b), we referred to this mode of recordings as "IN-CELL recordings" rather than as intracellular recordings. The amplitudes of IN-CELL recorded APs generated by a single *Aplysia* neuron's cell body (∼80 μm in diameter) that adhere to an array of gMμEs ranged from 2 to 30 mV. This range mainly reflected variabilities in the seal resistance formed between individual gMμEs and the cell body. Time-locked, evoked electrotonic EPSPs of up to 5 mV were also recorded from a network

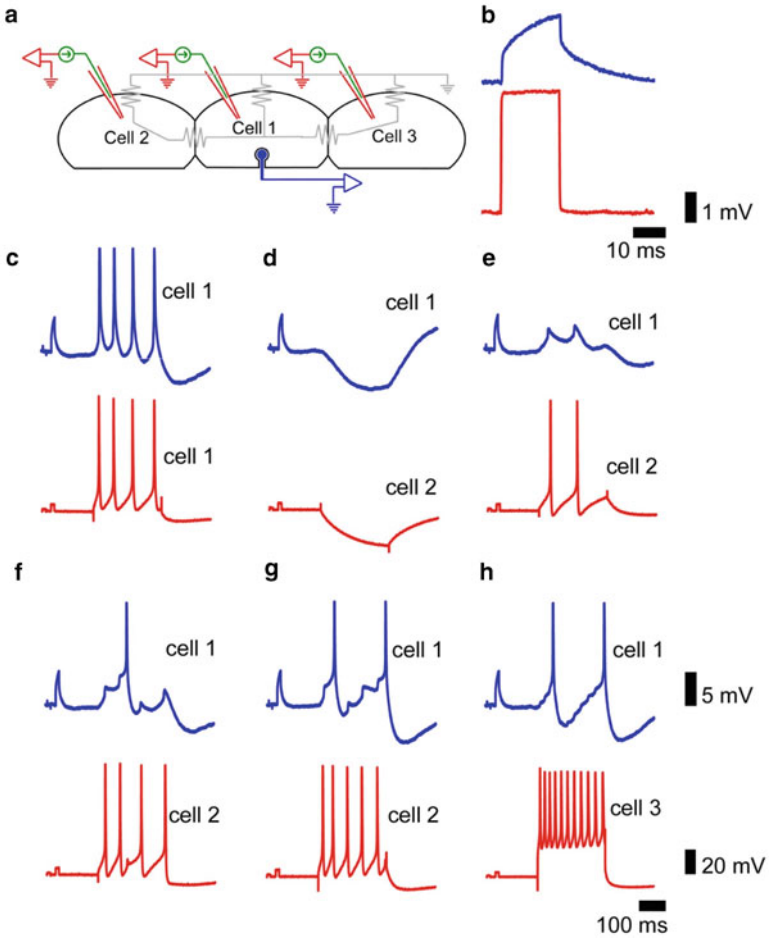

Fig. 9 Synaptic potentials and action potentials (APs) recorded by gold mushroom-shaped microelectrodes. (**a**) Three cells were cultured on a gMμE array. A single sharp intracellular microelectrode was used for both current injection and voltage recordings. (**b**) A calibration pulse of 5 mV, 20 ms as detected by the intracellular microelectrode (red) and a gMμE (blue). (**c**) Depolarization of neuron 1 generated a train of spikes recorded by the intracellular microelectrode (red in cell 1) and the gMμE (blue of cell 1). (**d**) The intracellular electrode was then moved into neuron 2. Hyperpolarization of neuron 2 generated hyperpolarization of neurons 2 and 1. (**e**) Depolarization of neuron 2 to generate two APs elicited two electrical EPSPs riding on the depolarizing pulse (blue) in neuron 1. (**f**, **g**) Increasing the strength of the intracellular stimulation of neuron 2 generated trains of 4 and 5 spikes in neuron 2 (correspondingly) leading to summation of the EPSPs in neuron 1, to fire one and two APs (**f**) and (**g**), correspondingly) as monitored by the gMμE from neuron 1. In (**h**), the intracellular electrode was moved into neuron 3. Spikes in cell 3 (red) also generate EPSPs which summated to generate action potentials in cell 1. (Reprinted with permission from Hai et al. (2010a). Copyright Nature Publishing Group 2010)

of electrically coupled neurons (Fig. 9 and Hai et al. 2010a, b). The use of an analog electrical circuit model to simulate the experimental results made it clear that the results were only possible if in addition to the increased seal resistance, the junctional membrane conductance was increased with respect to the non-junctional membrane. The mechanisms underlying this junctional membrane conductance increase remained unclear. It is conceivable that the curvature of the gMμE cap and/or the presence of the RGD repeat peptide on the electrode surface may have initiated a molecular cascade leading to recruitment of voltage independent ionic channels to the junctional membrane or to the formation of nanopores within the confined region of the junctional membrane.

The studies conducted using cultured *Aplysia* neurons revealed that the neuron–gMμE junctions were stable for approximately 2 weeks and that the neuron–gMμE hybrid configuration did not alter the passive or active membrane properties of the neurons and their synaptic functions (Hai et al. 2009b, 2010a, b).

The results obtained using gMμE-based MEA to record from primary cultures of rat hippocampal neurons differed in a number of ways from those of *Aplysia* neurons.

In contrast to cultured *Aplysia* neurons, the variability in the shapes and amplitude of the recorded potentials from cultured rat hippocampal neurons was significantly larger (Fig. 10), and ranged from biphasic extracellular FPs with amplitudes of 100 μV to positive monophasic 1–5 mV APs with characteristic features of juxtacellular recordings (Fig 10b) or intracellular recordings

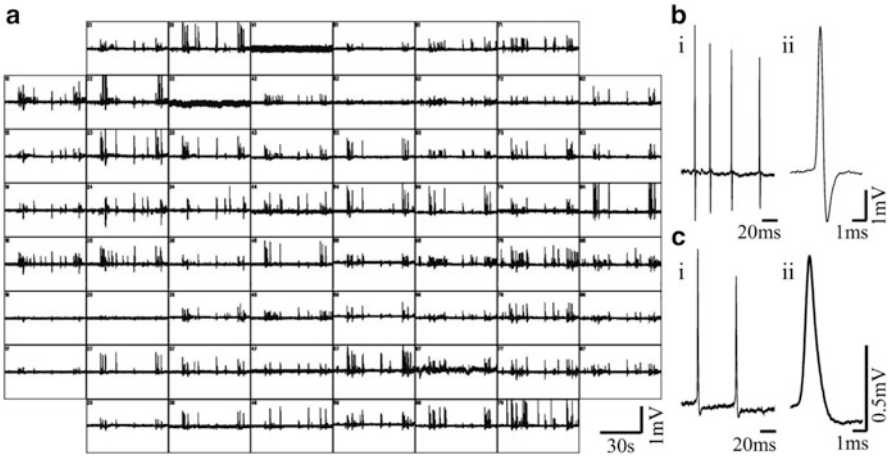

Fig. 10 Spontaneous activity recorded by 60 gMμE-MEA from cultured hippocampal neurons 17 DIV (**a**). Each box represents 30 s of recording from a single gMμE. Note that the majority of the gMμEs recorded monophasic positive action potentials (**b–c**) Enlargement of recorded APs by two gMμEs. Whereas in (**b**) the AP features are of loose seal-like configuration, that of (**c**) is of IN-CELL recordings. (Reprinted with permission from Shmoel et al. (2016). Copyright Nature Publishing Group, 2016)

(Fig. 10c and Shmoel et al. 2016). The large variability can be attributed to two factors. Because of the small diameter of hippocampal neuron cell bodies (15–20 μm), the probability of a neuron to be positioned optimally to engulf a gMμE and form a high seal resistance junction is lower than for the large diameter *Aplysia* neurons. In addition, the short duration of the recorded action potentials (by a fraction of the electrodes Fig. 10) suggest that in these cases the junctional membrane resistance is high. Under these conditions the electrical coupling between the neuron and the gMμE is capacitive rather than Ohmic. Thus, the shapes of the recorded APs resemble the time derivative of the genuine intracellular AP. The range of interfacing modes can be explained by the analog electrical circuits shown in Fig. 1a, b.

The circuits depicted by Fig. 1 illustrate two junctional membrane modes. In Fig. 1b, R_{jm} is large, >100 GΩ. Thus, the resistive component of the junctional membrane could be neglected and the membrane is represented by a capacitor (C_{jm}) with a value that corresponded to its surface area times 1 μF/cm^2. This together with the seal resistance formed by the cleft between the plasma membrane and the gMμE configures a passive electrical differentiator that generated an output potential proportional to the time derivative of the input (Rizzoni 2009). In contrast, if R_{jm} is low (∼1 GΩ) the circuit properties are transformed from a differentiator (Fig. 1b) to an element that does not distort the shape of the wave form (Fig. 1a). These changes corresponded to the transition between a loose seal/juxtacellular recording configuration and an IN-CELL recording. In fact, the changes in the relationships between the R_{jm} and C_{jm} are expected to generate a continuous spectrum of outputs ranging from juxtacellular to IN-CELL recording modes as

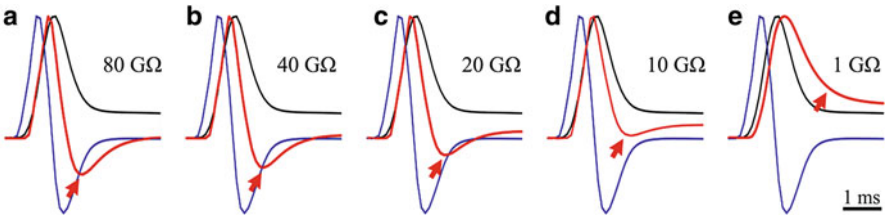

Fig. 11 Simulation of the shapes and amplitudes of action potentials as a function of the junctional membrane resistances using the analog electrical circuits of Fig. 1 and the analog electronic circuit simulator SPICE. The normalized input action-potential (black), its calculated time derivative (blue) and the simulated output (red) for R_{jm} values of 80-1 GΩ (as indicated). The shape of the output action potentials (red) changes (red arrow) from being similar to the time derivative of the input potential (**a**), gradually (**b** and **c**) to an intracellular recording (**d**, **e**). Aside from the dependence of the normalized simulated output shape, the increase in R_{jm} value is associated with a decrease in the amplitude of the simulated output AP, a change in the simulated AP duration, and a shift in the AP peak time with respect to the input AP (not shown for additional details see Shmoel et al. (2016) (Reprinted with permission from Shmoel et al. (2016). Copyright Nature Publishing Group, 2016)

illustrated by simulation of the analog electrical circuits of Fig. 1 (using the general-purpose, analog electronic circuit simulator SPICE) and shown by Fig. 11 (Shmoel et al. 2016).

Interestingly, contrary to what was found in *Aplysia*, the electrical coupling levels and mode of recording formed between hippocampal neurons and gMμEs were not improved by functionalizing the gMμE with the RGD repeat peptide. Ultrastructural observations by our lab and others have revealed that hippocampal neurons (and cardiomyocytes) engulf to tightly interface with gMμEs functionalized by poly-L-lysine or polyethyleneimine/laminin, suggesting that the 3D structure in itself (mushroom, and in fact also vertical nanoelectrodes) is sufficient to facilitate the engulfment (Fendyur et al. 2011; Santoro et al. 2013, 2014a, b; Ojovan et al. 2015; Shmoel et al. 2016; Zhao et al. 2017). Hence, it is conceivable that the expected effects of the RGD repeat peptide on the junctional membrane conductance of hippocampal neurons are not expressed by the time the hippocampal network matures its electrophysiological functions 10–14 days after plating. It is assumed that the peptide layers at the gold electrode surface undergo a degradation process by enzymes secreted by the neurons or by hydrolysis. Attempts to achieve Ohmic contact between gMμEs and the neurons by electroporation were unsuccessful. We observed that the hippocampal neurons–gMμE hybrids remained stable in culture for periods of up to 10 days. We have not yet tested whether gMμEs alter the physiological properties of the neurons or the network.

9 Recordings of Synaptic Potentials by Gold Mushroom-Shaped MEA?

In a number of experiments, we observed the presence of low amplitude (~100 μV) negative and positive potentials with slower rise and decay times than the APs (Fig. 12). Given that FPs generated by single neurons in culture decay to a third of their amplitude within a distance of approximately 100 μm (Weir et al. 2014), these potentials may reflect the pickup of FPs generated by remote neurons. Alternatively, these potentials could reflect a barrage of genuine excitatory and inhibitory synaptic potentials. Currently we cannot unequivocally differentiate between these possibilities by rigid criteria. Nevertheless, pharmacological experiments support the hypothesis that these are synaptic potentials. Specifically, the application of GABAzine, a GABAergic postsynaptic blocking reagent (1–10 μM), transformed the endogenous FPs firing pattern into typical bursts (Fig. 12a, b, respectively). Concomitantly, it led to the disappearance of the slow negative-going potentials (Fig. 12d, f). Hence, if the slow low-amplitude negative-going potentials had been generated by bursts of APs produced by remote neurons, the frequency and amplitude of the negative potentials would have increased rather than disappeared.

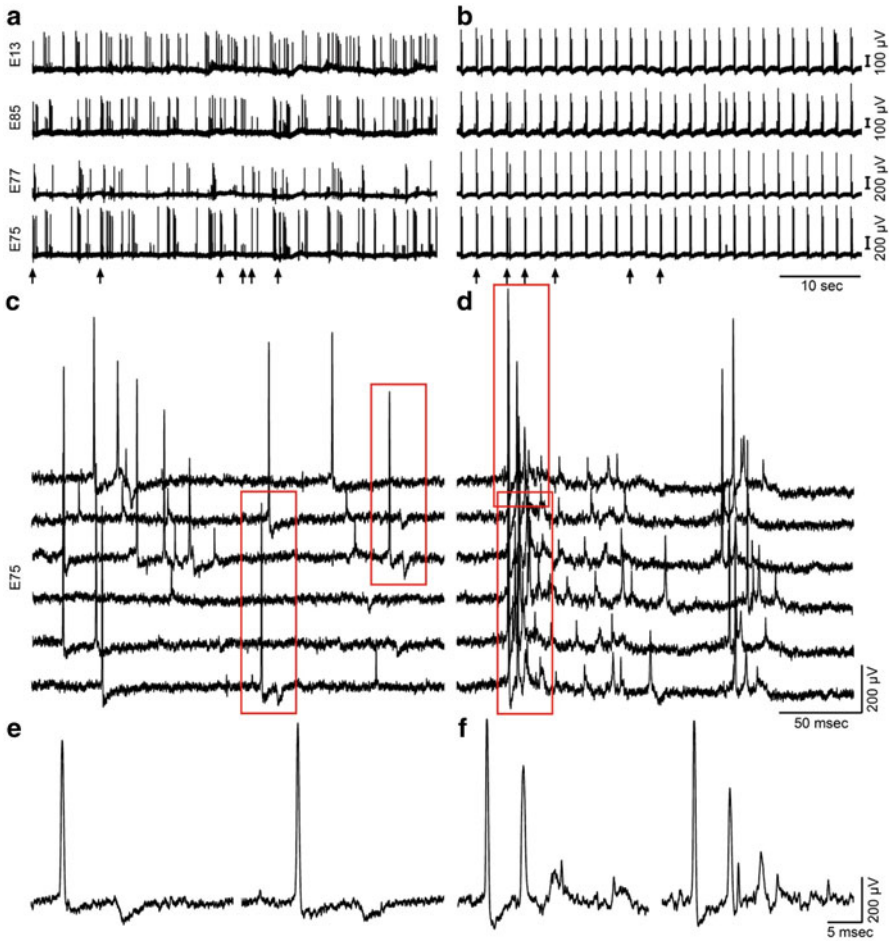

Fig. 12 The effect of GABAzine on recorded spontaneous electrophysiological signaling repertoire. Spontaneous firing as recorded by 4 gMμE before (**a**, **c**) and after the application of 10 μM GABAzine to the culture medium (**b**, **d**). (**c**, **d**) are enlargements of the bursts indicated by arrows in (**a**) and (**b**) respectively. (**e**, **f**) Enlargements of the potentials enclosed by red boxes in (**c**) and (**d**) respectively. GABAzine alters the spike firing pattern to distinct bursts. (**e**) The low-amplitude, long-duration negative potentials recorded before GABAzine application disappear after GABAzine application, and positive, but low-amplitude, long-duration potentials are recorded (**f**). These potentials are tentatively considered to be synaptic. The spikelets are possibly dendritic spikes or the firing of electronically coupled neurons. (Reprinted with permission from Shmoel et al. (2016). Copyright Nature Publishing Group, 2016)

In summary, the electrophysiological and pharmacological observations are consistent with the possibility that the relatively slow low-amplitude potentials recorded by the gMμEs from an in vitro network of hippocampal neurons could represent synaptic potentials.

10 Conclusions

Taken together, the results discussed in this chapter show at a proof-of-concept level that passive and active vertical nanoelectrodes can record attenuated intracellular spikes and subthreshold synaptic potentials from cultured neurons, cardiomyocytes, and skeletal myotubes. The attenuation of the recorded signals is mainly the outcome of the high impedance of the 3D vertical nanoelectrodes due to their small surface area. This could be improved by the use of nano-FETs rather than passive electrodes and the development of novel materials for electrode construction. Another shortcoming of currently used vertical nanoelectrode technology is the low seal resistance formed between the electrode and the cell. This parameter could be substantially improved by developing suitable surface chemistries to effectively fuse the electrodes with the cell's plasma membrane. The limited time, of approximately 1 h, during which intracellular recordings can be obtained after electroporation or optoporation is yet another aspect that should be improved. It is conceivable that slowdown of innate membrane repair mechanism which serves to protect cells from damage after membrane poration can be theoretically designed.

To conclude, the 10-year-old technologies of intracellular electrophysiological recordings from individual cells comprising cellular networks have made tremendous progress. It is foreseen that the use of the novel vertical nanoelectrodes-based MEA technologies that enable to read the entire electrophysiological signaling repertoire from individual cells within an operational network will have a significant impact on the progress of basic and applied brain research.

References

Abbott, J., Ye, T., Ham, D., & Park, H. (2018). Optimizing nanoelectrode arrays for scalable intracellular electrophysiology. *Accounts of Chemical Research, 51*, 600–608.

Abbott, J., Ye, T., Qin, L., Jorgolli, M., Gertner, R. S., Ham, D., et al. (2017). CMOS nanoelectrode array for all-electrical intracellular electrophysiological imaging. *Nature Nanotechnology, 12*, 460–466.

Almquist, B. D., & Melosh, N. A. (2010). Fusion of biomimetic stealth probes into lipid bilayer cores. *Proceedings of the National Academy of Sciences of the United States of America, 107*, 5815–5820.

Almquist, B. D., & Melosh, N. A. (2011). Molecular structure influences the stability of membrane penetrating biointerfaces. *Nano Letters, 11*, 2066–2070.

Almquist, B. D., Verma, P., Cai, W., & Melosh, N. A. (2011). Nanoscale patterning controls inorganic-membrane interface structure. *Nanoscale, 3*, 391–400.

Amin, H., Maccione, A., Marinaro, F., Zordan, S., Nieus, T., & Berdondini, L. (2016). Electrical responses and spontaneous activity of human iPS-derived neuronal networks characterized for 3-month culture with 4096-electrode arrays. *Frontiers in Neuroscience, 10*, 121.

Angle, M. R., Cui, B., & Melosh, N. A. (2015). Nanotechnology and neurophysiology. *Current Opinion in Neurobiology, 32*, 132–140.

Angle, M. R., & Schaefer, A. T. (2012). Neuronal recordings with solid-conductor intracellular nanoelectrodes (SCINEs). *PLoS One, 7*, e43194.

Angle, M. R., Wang, A., Thomas, A., Schaefer, A. T., & Melosh, N. A. (2014). Penetration of cell membranes and synthetic lipid bilayers by nanoprobes. *Biophysical Journal, 107*, 2091–2100.

Barth, A. L., & Poulet, J. F. (2012). Experimental evidence for sparse firing in the neocortex. *Trends in Neurosciences, 35*, 345–355.

Berdondini, L., Imfeld, K., Maccione, A., Tedesco, M., Neukom, S., Koudelka-Hep, M., et al. (2009a). Active pixel sensor array for high spatio-temporal resolution electrophysiological recordings from single cell to large scale neuronal networks. *Lab on a Chip, 9*, 2644–2651.

Berdondini, L., Massobrio, P., Chiappalone, M., Tedesco, M., Imfeld, K., Maccione, A., et al. (2009b). Extracellular recordings from locally dense microelectrode arrays coupled to dissociated cortical cultures. *Journal of Neuroscience Methods, 177*, 386–396.

Berdondini, L., Van Der Wal, P. D., Guenat, O., De Rooij, N. F., Koudelka-Hep, M., Seitz, P., et al. (2005). High-density electrode array for imaging in vitro electrophysiological activity. *Biosensors and Bioelectronics, 21*, 167–174.

Braeken, D., Jans, D., Huys, R., Stassen, A., Collaert, N., Hoffman, L., et al. (2012). Open-cell recording of action potentials using active electrode arrays. *Lab on a Chip, 12*, 4397–4402.

Braun, D., & Fromherz, P. (1998). Fluorescence interferometry of neuronal cell adhesion on microstructured silicon. *Physical Review Letters, 81*, 5241–5244.

Chernomordik, L. V., & Kozlov, M. M. (2008). Mechanics of membrane fusion. *Nature Structural and Molecular Biology, 15*, 675–683.

Claycomb, W. C., Lanson Jr., N. A., Stallworth, B. S., Egeland, D. B., Delcarpio, J. B., Bahinski, A., et al. (1998). HL-1 cells: A cardiac muscle cell line that contracts and retains phenotypic characteristics of the adult cardiomyocyte. *Proceedings of the National Academy of Sciences of the United States of America, 95*, 2979–2984.

Cohen, A., Shappir, J., Yitzchaik, S., & Spira, M. E. (2008). Reversible transition of extracellular field potential recordings to intracellular recordings of action potentials generated by neurons grown on transistors. *Biosensors and Bioelectronics, 23*, 811–819.

De Angelis, F., Malerba, M., Patrini, M., Miele, E., Das, G., Toma, A., et al. (2013). 3D hollow nanostructures as building blocks for multifunctional plasmonics. *Nano Letters, 13*, 3553–3558.

Demonbreun, A. R., & Mcnally, E. M. (2016). Plasma membrane repair in health and disease. *Current Topics in Membranes, 77*, 67–96.

Dipalo, M., Amin, H., Lovato, L., Moia, F., Caprettini, V., Messina, G. C., et al. (2017). Intracellular and extracellular recording of spontaneous action potentials in mammalian neurons and cardiac cells with 3D plasmonic nanoelectrodes. *Nano Letters, 17*, 3932–3939.

Dipalo, M., Messina, G. C., Amin, H., La Rocca, R., Shalabaeva, V., Simi, A., et al. (2015). 3D plasmonic nanoantennas integrated with MEA biosensors. *Nanoscale, 7*, 3703–3711.

Duan, X., Gao, R., Xie, P., Cohen-Karni, T., Qing, Q., Choe, H. S., et al. (2012). Intracellular recordings of action potentials by an extracellular nanoscale field-effect transistor. *Nature Nanotechnology, 7*, 174–179.

Epand, R. M., D'souza, K., Berno, B., & Schlame, M. (2015). Membrane curvature modulation of protein activity determined by NMR. *Biochimica et Biophysica Acta, 1848*, 220–228.

Epsztein, J., Brecht, M., & Lee, A. K. (2011). Intracellular determinants of hippocampal CA1 place and silent cell activity in a novel environment. *Neuron, 70*, 109–120.

Fekete, Z. (2015). Recent advances in silicon-based neural microelectrodes and microsystems: A review. *Sensors and Actuators B: Chemical, 215*, 300–315.

Fendyur, A., Mazurski, N., Shappir, J., & Spira, M. E. (2011). Formation of essential ultrastructural interface between cultured hippocampal cells and gold mushroom-shaped MEA-toward "IN-CELL" recordings from vertebrate neurons. *Frontiers in Neuroengineering, 4*, 14.

Fendyur, A., & Spira, M. E. (2012). Toward on-chip, in-cell recordings from cultured cardiomyocytes by arrays of gold mushroom-shaped microelectrodes. *Frontiers in Neuroengineering, 5*, 21.

Fromherz, P. (2003). *Neuroelectronic interfacing: Semiconductor chips with ion channels, nerve cells, and brain*. Berlin: Wiley-VCH.

Gao, R., Strehle, S., Tian, B., Cohen-Karni, T., Xie, P., Duan, X., et al. (2012). Outside looking in: Nanotube transistor intracellular sensors. *Nano Letters, 12*, 3329–3333.

Gold, C., Girardin, C. C., Martin, K. A., & Koch, C. (2009). High-amplitude positive spikes recorded extracellularly in cat visual cortex. *Journal of Neurophysiology, 102*, 3340–3351.

Hai, A., Dormann, A., Shappir, J., Yitzchaik, S., Bartic, C., Borghs, G., et al. (2009a). Spine-shaped gold protrusions improve the adherence and electrical coupling of neurons with the surface of micro-electronic devices. *Journal of the Royal Society Interface, 6*, 1153–1165.

Hai, A., Kamber, D., Malkinson, G., Erez, H., Mazurski, N., Shappir, J., et al. (2009b). Changing gears from chemical adhesion of cells to flat substrata toward engulfment of micro-protrusions by active mechanisms. *Journal of Neural Engineering, 6*, 066009.

Hai, A., Shappir, J., & Spira, M. E. (2010a). In-cell recordings by extracellular microelectrodes. *Nature Methods, 7*, 200–202.

Hai, A., Shappir, J., & Spira, M. E. (2010b). Long-term, multisite, parallel, in-cell recording and stimulation by an array of extracellular microelectrodes. *Journal of Neurophysiology, 104*, 559–568.

Hai, A., & Spira, M. E. (2012). On-chip electroporation, membrane repair dynamics and transient in-cell recordings by arrays of gold mushroom-shaped microelectrodes. *Lab on a Chip, 12*, 2865–2873.

Han, R., & Campbell, K. P. (2007). Dysferlin and muscle membrane repair. *Current Opinion in Cell Biology, 19*, 409–416.

Hanson, L., Lin, Z. C., Xie, C., Cui, Y., & Cui, B. X. (2012). Characterization of the cell-nanopillar interface by transmission electron microscopy. *Nano Letters, 12*, 5815–5820.

Hille, B. (1992). *Ionic channels of excitable membranes*. Sunderland: Sinauer.

Horn, R., & Marty, A. (1988). Muscarinic activation of ionic currents measured by a new whole-cell recording method. *The Journal of General Physiology, 92*, 145–159.

Iversen, L., Mathiasen, S., Larsen, J. B., & Stamou, D. (2015). Membrane curvature bends the laws of physics and chemistry. *Nature Chemical Biology, 11*, 822–825.

Jackel, D., Bakkum, D. J., Russell, T. L., Muller, J., Radivojevic, M., Frey, U., et al. (2017). Combination of high-density microelectrode array and patch clamp recordings to enable studies of multisynaptic integration. *Scientific Reports, 7*, 978.

Jenkner, M., & Fromherz, P. (1997). Bistability of membrane conductance in cell adhesion observed in a neuron transistor. *Physical Review Letters, 79*, 4705–4708.

Joshi, R. P., & Schoenbach, K. H. (2002). Mechanism for membrane electroporation irreversibility under high-intensity, ultrashort electrical pulse conditions. *Physical Review. E, Statistical, Nonlinear, and Soft Matter Physics, 66*, 052901.

Joshi, S., & Hawken, M. J. (2006). Loose-patch-juxtacellular recording in vivo—a method for functional characterization and labeling of neurons in macaque V1. *Journal of Neuroscience Methods, 156*, 37–49.

Jun, J. J., Steinmetz, N. A., Siegle, J. H., Denman, D. J., Bauza, M., Barbarits, B., et al. (2017). Fully integrated silicon probes for high-density recording of neural activity. *Nature, 551*, 232–236.

Lefler, Y., Yarom, Y., & Uusisaari, M. Y. (2014). Cerebellar inhibitory input to the inferior olive decreases electrical coupling and blocks subthreshold oscillations. *Neuron, 81*, 1389–1400.

Lin, Z. C., & Cui, B. (2014). Nanowire transistors: Room for manoeuvre. *Nature Nanotechnology, 9*, 94–96.

Lin, Z. C., Xie, C., Osakada, Y., Cui, Y., & Cui, B. (2014). Iridium oxide nanotube electrodes for sensitive and prolonged intracellular measurement of action potentials. *Nature Communications, 5*, 3206.

Liu, R., Chen, R., Elthakeb, A. T., Lee, S. H., Hinckley, S., Khraiche, M. L., et al. (2017). High density individually addressable nanowire arrays record intracellular activity from primary rodent and human stem cell derived neurons. *Nano Letters, 17*, 2757–2764.

Lou, H. Y., Zhao, W., Zeng, Y., & Cui, B. (2018). The role of membrane curvature in nanoscale topography-induced intracellular signaling. *Accounts of Chemical Research, 51*, 1046–1053.

Massobrio, G., Martinoia, S., & Massobrio, P. (2018). Equivalent circuit of the neuro-electronic junction for signal recordings from planar and engulfed micro-nano-electrodes. *IEEE Transactions on Biomedical Circuits and Systems, 12*, 3–12.

Massobrio, P., Massobrio, G., & Martinoia, S. (2016). Interfacing cultured neurons to microtransducers arrays: A review of the neuro-electronic junction models. *Frontiers in Neuroscience, 10*, 282.

Mcneil, P. L., & Khakee, R. (1992). Disruptions of muscle fiber plasma membranes. Role in exercise-induced damage. *The American Journal of Pathology, 140*, 1097–1109.

Mcneil, P. L., & Kirchhausen, T. (2005). An emergency response team for membrane repair. *Nature Reviews. Molecular Cell Biology, 6*, 499–505.

Messina, G. C., Dipalo, M., La Rocca, R., Zilio, P., Caprettini, V., Zaccaria, R. P., et al. (2015). Spatially, temporally, and quantitatively controlled delivery of broad range of molecules into selected cells through plasmonic nanotubes. *Advanced Materials, 27*, 7145–7149.

Obien, M. E., Deligkaris, K., Bullmann, T., Bakkum, D. J., & Frey, U. (2014). Revealing neuronal function through microelectrode array recordings. *Frontiers in Neuroscience, 8*, 423.

Ojovan, S. M., Rabieh, N., Shmoel, N., Erez, H., Maydan, E., Cohen, A., et al. (2015). A feasibility study of multi-site, intracellular recordings from mammalian neurons by extracellular gold mushroom-shaped microelectrodes. *Scientific Reports, 5*, 14100.

Oren, R., Sfez, R., Korbakov, N., Shabtai, K., Cohen, A., Erez, H., et al. (2004). Electrically conductive 2D-PAN-containing surfaces as a culturing substrate for neurons. *Journal of Biomaterials Science. Polymer Edition, 15*, 1355–1374.

Qing, Q., Jiang, Z., Xu, L., Gao, R. X., Mai, L. Q., & Lieber, C. M. (2014). Free-standing kinked nanowire transistor probes for targeted intracellular recording in three dimensions. *Nature Nanotechnology, 9*, 142–147.

Rabieh, N., Ojovan, S. M., Shmoel, N., Erez, H., Maydan, E., & Spira, M. E. (2016). On-chip, multisite extracellular and intracellular recordings from primary cultured skeletal myotubes. *Scientific Reports, 6*, 36498.

Rizzoni, G. (2009). *Fundamentals of electrical engineering*. New York: McGraw-Hill.

Robinson, J. T., Jorgolli, M., Shalek, A. K., Yoon, M. H., Gertner, R. S., & Park, H. (2012). Vertical nanowire electrode arrays as a scalable platform for intracellular interfacing to neuronal circuits. *Nature Nanotechnology, 7*, 180–184.

Sackmann, E., & Bruinsma, R. F. (2002). Cell adhesion as wetting transition? *Chemphyschem, 3*, 262–269.

Sakmann, B., & Neher, E. (1984). Patch clamp techniques for studying ionic channels in excitable membranes. *Annual Review of Physiology, 46*, 455–472.

Santoro, F., Dasgupta, S., Schnitker, J., Auth, T., Neumann, E., Panaitov, G., et al. (2014a). Interfacing electrogenic cells with 3D nanoelectrodes: Position, shape, and size matter. *ACS Nano, 8*, 6713–6723.

Santoro, F., Panaitov, G., & Offenhausser, A. (2014b). Defined patterns of neuronal networks on 3D thiol-functionalized microstructures. *Nano Letters, 14*, 6906–6909.

Santoro, F., Schnitker, J., Panaitov, G., & Offenhäusser, A. (2013). On chip guidance and recording of cardiomyocytes with 3D mushroom-shaped electrodes. *Nano Letters, 13*, 5379–5384.

Santoro, F., Zhao, W., Joubert, L. M., Duan, L., Schnitker, J., Van De Burgt, Y., et al. (2017). Revealing the cell-material interface with nanometer resolution by focused ion beam/scanning electron microscopy. *ACS Nano, 11*, 8320–8328.

Seymour, J., Wu, F., Wise, K. D., & Yoon, E. (2017). State-of-the-art MEMS and microsystem tools for brain research. *Microsystems and Nanoengineering, 3*, 1–16.

Shmoel, N., Rabieh, N., Ojovan, S. M., Erez, H., Maydan, E., & Spira, M. E. (2016). Multisite electrophysiological recordings by self-assembled loose-patch-like junctions between cultured hippocampal neurons and mushroom-shaped microelectrodes. *Scientific Reports, 6*, 27110.

Shoham, S., O'connor, D. H., & Segev, R. (2006). How silent is the brain: Is there a "dark matter" problem in neuroscience? *Journal of Comparative Physiology. A, Neuroethology, Sensory, Neural, and Behavioral Physiology, 192*, 777–784.

Sileo, L., Pisanello, F., Quarta, L., Maccione, A., Simi, A., Berdondini, L., et al. (2013). Electrical coupling of mammalian neurons to microelectrodes with 3D nanoprotrusions. *Microelectronic Engineering, 111*, 384–390.

Spira, M. E., & Hai, A. (2013). Multi-electrode array technologies for neuroscience and cardiology. *Nature Nanotechnology, 8*, 83–94.

Spira, M. E., Kamber, D., Dormann, A., Cohen, A., Bartic, C., Borghs, G., et al. (2007). Improved neuronal adhesion to the surface of electronic device by engulfment of protruding micro-nails fabricated on the chip surface. *Transducers and Eurosensors, 1*, 1247–1250.

Thomas Jr., C. A., Springer, P. A., Loeb, G. E., Berwald-Netter, Y., & Okun, L. M. (1972). A miniature microelectrode array to monitor the bioelectric activity of cultured cells. *Experimental Cell Research, 74*, 61–66.

Tian, B., Cohen-Karni, T., Qing, Q., Duan, X., Xie, P., & Lieber, C. M. (2010). Three-dimensional, flexible nanoscale field-effect transistors as localized bioprobes. *Science, 329*, 830–834.

VanDersal, J. J., & Renaud, P. (2016). Biomimetic surface patterning for long-term transmembrane access. *Scientific Reports, 6*, 32485.

Verma, P., Wong, I. Y., & Melosh, N. A. (2010). Continuum model of mechanical interactions between biological cells and artificial nanostructures. *Biointerphases, 5*, 37–44.

Viswam, V., Bounik, R., Shadmani, A., Dragas, J., Obien, M., Muller, J., et al. (2017). High-density mapping of brain slices using a large multi-functional high-density CMOS microelectrode array system. *International Solid State Sensors Actuators and Microsystems Conference, 2017*, 135–138.

Weir, K., Blanquie, O., Kilb, W., Luhmann, H. J., & Sinning, A. (2014). Comparison of spike parameters from optically identified GABAergic and glutamatergic neurons in sparse cortical cultures. *Frontiers in Cellular Neuroscience, 8*, 460.

Weis, R., & Fromherz, P. (1997). Frequency dependent signal-transfer in neuron-transistors. *Physical Review E, 55*, 877–889.

Wise, K. D., Angell, J. B., & Starr, A. (1970). An integrated-circuit approach to extracellular microelectrodes. *IEEE Transactions on Biomedical Engineering, 17*, 238–247.

Xie, C., Lin, Z., Hanson, L., Cui, Y., & Cui, B. (2012). Intracellular recording of action potentials by nanopillar electroporation. *Nature Nanotechnology, 7*, 185–190.

Xu, A. M., Aalipour, A., Leal-Ortiz, S., Mekhdjian, A. H., Xie, X., Dunn, A. R., et al. (2014). Quantification of nanowire penetration into living cells. *Nature Communications, 5*, 3613.

Zeck, G., & Fromherz, P. (2003). Repulsion and attraction by extracellular matrix protein in cell adhesion studied with nerve cells and lipid vesicles on silicon chips. *Langmuir, 19*, 1580–1585.

Zhao, W., Hanson, L., Lou, H. Y., Akamatsu, M., Chowdary, P. D., Santoro, F., et al. (2017). Nanoscale manipulation of membrane curvature for probing endocytosis in live cells. *Nature Nanotechnology, 12*, 750–756.

Zilio, P., Dipalo, M., Tantussi, F., Messina, G. C., & De Angelis, F. (2017). Hot electrons in water: Injection and ponderomotive acceleration by means of plasmonic nanoelectrodes. *Light-Science and Applications, 6*(6), e17002.